Mathematical modelling of contact lens moulding

ELLEN A. MURPHY AND WILLIAM T. LEE
MACSI, Department of Mathematics and Statistics,
University of Limerick, Ireland.

accepted: 14 December, 2016

Abstract

Compression moulded contact lenses are produced by placing fluid between two moulds and squeezing the fluid outwards to form the shape of the lens. A common problem seen in this process is that at times the fluid moves outwards asymmetrically, resulting in partially formed lenses. In this paper, the system is modelled using the thin film equations and the results are analysed to find the optimal operating setup to reduce asymmetrical flow. A simple model with one curved surface and one flat surface is considered first. This assumption is verified by a more realistic model that investigates the effects of curvature on the dynamics of the fluid. The simple model is modified to include the effect of surface tension. The results of this model show that surface tension plays no role in the fluid dynamics for this particular fluid. A second modified model allows for lateral movement of the lower mould. The model shows that allowing the lower mould to slide hinders the symmetrical flow of the fluid. Contact lens; thin film; lubrication theory

1 Introduction

A contact lens is a thin lens that is placed on the surface of the eye, either to correct vision or to alter the appearance of the eye. One method of manufacturing contact lenses is compression moulding (Neefe, 1979; Dweib and Ó Bradaigh, 2000; Yamauchi et al., 2002). Two moulds are shaped so that when one is placed

on top of the other, the gap between them is the shape of the contact lens. Fluid is placed in the lower mould and the upper mould is pushed down onto it. This squeezes the fluid, causing it to flow outwards and fill the gap between the two moulds.

A squeeze layer occurs when a thin layer of fluid is placed between two surfaces and a normal force is applied. There have been extensive experimental and theoretical studies on squeeze layers. Mathematical modelling has been applied to a tear film over a contact lens (Talbott et al., 2014), but not to the moulding of contact lenses. A general review of modelling squeeze layers is given by Engmann et al. (2005), viscoelastic fluids are examined by Leider and Bird (1974) and Venerus et al. (2000) and fluids with wall slip are analysed by Lawal and Kalyon (2000). In this particular system, the squeeze layer occurs in a curved geometry, making it very similar to the well-known problem of lubrication in journal bearings. For an introduction to modelling flow in journal bearings see chapter 7 in Cameron and Mc Ettles (1976). Another example of a squeeze layer in a curved geometry is the lubrication of physiological joints (see Medley et al., 1984; Walicki and Walicka, 2000; Ruggiero et al., 2011).

Squeeze layers are generally modelled using the thin film equations, otherwise known as the lubrication approximation, which were developed by Reynolds (1886) on the foundation of work done by Stefan (1874). The thin film equations are applied when there are two significantly different length scales in the problem. There have been many studies of thin film flow on curved surfaces, in particular the modelling of coating flows where surface tension effects are often important. See, for example, Bretherton (1961); Jensen (1997); Roy et al. (2002); Howell (2003), and the references therein.

The motivation for this paper is a commonly seen problem in the compression moulding process. In some cases, the fluid does not spread outwards symmetrically and uniformly, as illustrated in figure 1. This causes some contact lenses to be only partially formed and consequently, rejected. We report the results of a modelling study of the phenomenon.

The aim of this study is to formulate a mathematical model to determine the factors contributing to asymmetrical flow and to develop recommendations to avoid it. Possible causes for asymmetrical flow include: an initially off-centred fluid; surface tension effects; and incorrect positioning of the lower mould. The model is developed to reflect these possible causes, investigating each of them in turn.

To model the system, the thin film equations are used. The pressure along the film is found for a given two-dimensional section. Once the pressure is known, the

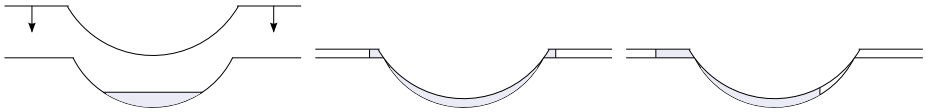

(a) Fluid is placed in the lower mould and the upper mould is then pushed down.

(b) Fully filled mould.

(c) Partially filled mould.

Figure 1: Schematic of the moulding process.

evolution of the position of the edges of the fluid can be determined. Of particular interest is whether or not the edges of the fluid move outwards symmetrically. The fluid moving outwards symmetrically implies that the contact lens will be formed correctly. Asymmetric flow suggests that the moulds will be partially filled and the resulting lens rejected.

As the main type of defect observed in the moulding process is the off-centring of monomer, we restrict our attention the simplest model in which off-centring can be observed: a planar two dimensional geometry. While this class of model does not allow us to address defects arising from complex flow patterns such as fingering, these are not observed in practice.

As a first approximation, a very simple model is developed where surface tension is neglected and the system is modelled as flat. That is, the curvature of the lower mould is absorbed into the curvature of the upper mould and the lower surface is considered flat. This simplification is then justified by a more realistic model, formulated in polar coordinates, where both surfaces are curved. The effects of including surface tension in the model are also investigated. The subject is concluded by investigating the effect of introducing lateral motion of the lower mould to the model. Results from each model are given, along with recommendations to prevent asymmetrical flow.

2 Geometry

The moulds are rigid, smooth and impermeable. The lower mould is fixed in place while the upper mould moves vertically, at a constant speed. The moulds are shaped like sections cut from a hollow sphere, as shown in figure 2. The curved part of the lower mould has a smaller radius of curvature than the curved part of the upper mould. When the upper mould is sitting on top of the lower mould, the

void between the two moulds is the shape of the contact lens.

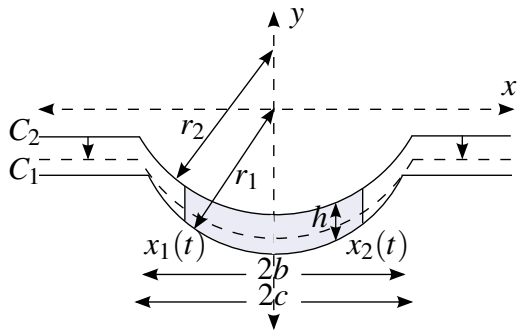

Figure 2: Schematic of the moulds and positions of the fluid boundaries. The lower mould, C_1, is fixed in place and has a curved middle section of radius r_1, for a width of $2b$. The upper mould, C_2, moves downwards on to the lower mould. Its curved section has a radius of r_2, for a width of $2c$. The free surfaces of the fluid are denoted x_1 and x_2. The height of the fluid is denoted h.

The vertical height between the two moulds is much less than the horizontal length of the moulds. The fluid in question is a highly viscous monomer and is assumed to be Newtonian. The parameter values of the fluid and the geometry are given in table 1. For the parameter values given, the modified Reynolds number for this problem is small and the lubrication approximation is appropriate. The system is modelled in two dimensions.

Figure 2 shows a schematic of the system. The setup consists of a lower mould, C_1, and an upper mould, C_2. Both moulds are of the form of truncated hemispheres joined to flat, horizontal sides. Fluid is placed in the lower mould and the upper mould is then pushed vertically down on to the lower mould at a constant speed, v_0. The circular part of the lower mould has radius of curvature r_1 and the upper mould has radius of curvature r_2, where $r_2 > r_1$. When the moulds make contact, the circle of intersection has a radius of b and the maximum vertical height between the moulds is h_0. As an approximation, the system is assumed to be axially symmetric and is modelled in two dimensions. The height of the fluid between moulds, h, is small relative to b, such that $h \ll b$. The positions of the lateral free surfaces or boundaries of the fluid are denoted $x = x_1(t)$ and $x = x_2(t)$, with $x_1 \leqslant x \leqslant x_2$.

3 Flat model

As a first approximation, we assume that from the perspective of the fluid, the mould is flat. Therefore, instead of considering two curved surfaces, $y = C_1(x)$ and $y = C_2(t,x)$, we consider one flat surface, $y = 0$, and one curved surface, $y = h(t,x)$, where $h(t,x) = C_2(t,x) - C_1(x)$, as displayed in figure 3. To reduce the complexity of the model, the equations for the moulds are chosen so that at $t = t_0 < 0$ they begin separate and then make contact at $t = 0$.

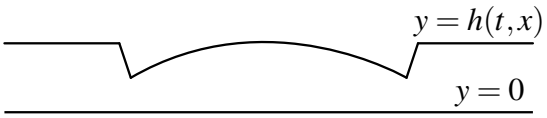

Figure 3: Geometry of the simple 'flat' model. Instead of two curved surfaces, the model has one flat surface, $y = 0$, and one curved surface, $y = h(t,x)$ (not to scale).

3.1 Governing equations

The governing equations are the Navier-Stokes equations with no-slip and no-flow boundary conditions on both surfaces. To nondimensionalise the system, the following scales are used:

$$x \sim b, \quad y \sim h_0, \quad h \sim h_0, \quad t \sim \frac{h_0}{v_0}, \quad u \sim \frac{v_0 b}{h_0}, \quad v \sim v_0, \quad p \sim \frac{\rho {v_0}^2}{\varepsilon^4 \mathrm{Re}}, \tag{31}$$

where u and v are the velocities in the x and y directions, respectively, p is the pressure, $\mathrm{Re} = \frac{\rho v_0 b^2}{\mu h_0}$ is the Reynolds number for the system, where μ is the dynamic viscosity. The velocity in the y direction is scaled with v_0 as this is a fixed quantity in the system. After nondimensionalisation the same notation for the dimensionless variables is retained. The parameter, ε, is the ratio of the two length scales and is small,

$$\varepsilon = \frac{h_0}{b} \approx 0.03 \ll 1, \tag{32}$$

and is used to simplify the equations. To first order, the dimensionless Navier-Stokes equations are the thin film equations (see, for example, Acheson, 1990).

At the free surfaces, x_i, the following conditions hold:

$$p(t,x_i) = 0, \qquad Q(t,x_i) = h(t,x_i)\dot{x}_i, \tag{33}$$

where Q is the volume flux and $i = 1,2$. These conditions describe the mass and momentum balance at the boundaries, in the absence of surface tension and evaporation.

Solving the thin film equations with the appropriate boundary conditions results in the Reynolds equation,

$$\frac{\partial h}{\partial t} = \frac{\partial}{\partial x}\left(\frac{h^3}{12}\frac{\partial p}{\partial x}\right) \qquad \text{in} \qquad (x_1,x_2). \tag{34}$$

Mass conservation implies that

$$\frac{\partial Q}{\partial x} = -\frac{\partial h}{\partial t}, \tag{35}$$

and given that $\frac{\partial h}{\partial t} = -1$, (35) can be integrated to give an expression for the flux,

$$Q = x - x_0(t), \tag{36}$$

where x_0 is determined below. The flux is also given by

$$Q = \int_0^h u \,\mathrm{d}y, \tag{37}$$

which results in a second expression for the flux,

$$Q = -\frac{h^3}{12}\frac{\partial p}{\partial x}. \tag{38}$$

Setting the two expressions for the flux equal to one another, and rearranging, gives an expression for the pressure gradient,

$$\frac{\partial p}{\partial x} = -\frac{12(x-x_0)}{h^3}, \tag{39}$$

such that $x_0(t)$ is the position of maximum pressure in the fluid film. This expression is integrated over x and the first condition in (33) is applied to give

$$x_0(t) = \frac{\int_{x_1}^{x_2} \frac{x}{h^3}\,\mathrm{d}x}{\int_{x_1}^{x_2} \frac{1}{h^3}\,\mathrm{d}x}. \tag{310}$$

Using (33) and (36), the ordinary differential equations (ODEs) for $x_1(t)$ and $x_2(t)$ are:

$$\dot{x}_1(t) = \frac{x_1(t) - x_0(t)}{h(t, x_1(t))}, \tag{311}$$

$$\dot{x}_2(t) = \frac{x_2(t) - x_0(t)}{h(t, x_2(t))}. \tag{312}$$

The ODEs are, qualitatively at least, what one would anticipate. The rates of change of the positions of the fluid boundaries increase with the distance between the fluid boundaries and the position of maximum pressure, and decrease with increasing height of the fluid at the boundaries.

Table 1: Values of constants used in simulations. The values were provided by the industrial contact.

Property	Parameter	Value
Radius of lower mould	r_1	8.5 mm
Radius of upper mould	r_2	8.8 mm
Radius of intersection	b	7.1 mm
Height between moulds when touching	h_0	0.226 mm
Density	ρ	0.98×10^3 kg m^{-3}
Surface tension	γ	27 mN m^{-1}
Dynamic viscosity	μ	2.5 Pa s
Velocity of upper mould	v_0	0.6 mm s^{-1}
Reynolds number (flat model)	Re	0.05
Reynolds number (curved model)	Re_p	0.02
Reduced inverse capillary number	λ	0.01 - 0.03

3.2 Initial conditions

The initial conditions for x_1 and x_2 are found numerically. This is done by choosing a value for the position of the centre of mass, x_{cm}, at the initial time, t_0, and then $x_1(t_0)$ and $x_2(t_0)$ are found such that they satisfy a given constant volume, $V = \int_{x_1}^{x_2} h \, \mathrm{d}x$. The volume is chosen to be 140% of the volume of the gap between the moulds when the two moulds are in contact. This is to replicate the commonly used procedure of overfilling the moulds.

3.3 Numerical results

The dimensionless system of ODEs, equations (311) and (312), is solved numerically. Due to the nature of the thin film equations, it would take an infinite amount of time to reduce the height of the fluid to zero. As such, the equations for the evolution of the free surfaces, (311) and (312), become singular as h approaches zero. Similarly, p and x_0 also become singular as h approaches zero. As a result of this, in all cases described below, the simulation is stopped when the minimum value of h is small but greater than zero. This limitation could be resolved by including surface roughness or by modelling the fluid on the molecular scale. However, as the phenomena of interest have occurred before h approaches zero, it is not necessary to do so for this system.

The results of the simulation using the parameter values given in table 1 are shown in figure 4. Figure 4a shows the evolution of the fluid boundaries and the centre of mass for an initially centred fluid, $x_{\mathrm{cm}}(t_0) = 0$. The fluid is initially centred on the lower mould and remains so as the moulds come closer together. No instability of the fluid is demonstrated. The fluid boundaries progress symmetrically and reach the flat part of the lower mould at $t \approx -1.1$.

A key question is whether initially off-centred doses of fluid remain off-centred when the upper mould is pushed down on the fluid. To investigate this, an initially off-centre positioned fluid was simulated. The fluid in figure 4b has an initial value of $x_{\mathrm{cm}} = 0.5$. As demonstrated by this figure, once the fluid is positioned asymmetrically, it remains this way, with no mechanism to realign it. It can be shown that the greater the initial misalignment of the fluid, the more asymmetrical the resulting flow. For $x_{\mathrm{cm}}(t_0) = 0.5$, both fluid boundaries are not past the curved section of the lower mould until $t \approx -0.5$.

Figure 4 also shows $x_{\mathrm{cm}}(t)$, the position of the centre of mass of the fluid, and $x_0(t)$, the position of maximum pressure, for both cases. For $x_{\mathrm{cm}}(t_0) = 0$, both variables remain at $x = 0$ as expected. For $x_{\mathrm{cm}}(t_0) = 0.5$, the evolution of these variables can be explained as follows. Starting with an initially off-centred fluid, h is approximately independent of x and hence the curves for x_0 and x_{cm} are reasonably flat. As the moulds approach each other, this is no longer true as h is now comparable to x. The fluid begins to feel a restoring force, pushing its centre of mass back towards $x = 0$. This exhibits itself in the dip in $x_{\mathrm{cm}}(t)$ and the increase in $x_0(t)$. Although it may not be clear from the figure, the gradient of $x_0(t)$ is positive until approximately $t = -2.5$ and the gradient of $x_{\mathrm{cm}}(t)$ is negative until approximately $t = -0.75$. As x_1 approaches the edge at $x = -1$, x_0 rapidly moves towards $x = 0$ and the fluid can now be thought of heuristically in

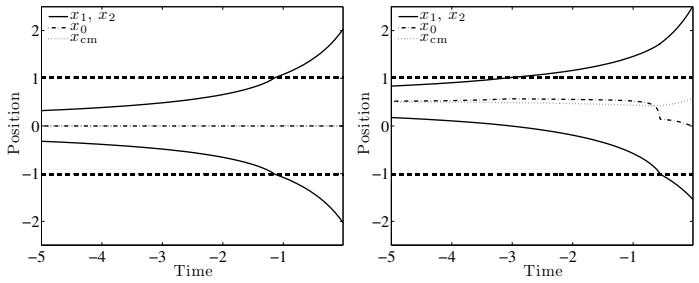

(a) $x_{cm}(t_0) = 0$. (b) $x_{cm}(t_0) = 0.5$.

Figure 4: Evolution of the fluid boundaries for the simple model. The dashed lines at positions 1 and -1 indicate where the lower mould changes from curved to flat.

two parts: a centred part, which proceeds symmetrically, as in figure 4a, and an off-centred part which moves further away from the centre.

The simulations show that once a fluid is centred, there is no mechanism to destabilise it and move it off-centre but if a fluid is initially off-centred it will remain so. The simulations suggest the system has marginal stability, i.e. an off-centred dose is neither pushed towards nor away from the centre. Please see appendix A for a more thorough analysis of the stability of the system.

4 Curved model

In the previous section, the system was modelled with one flat surface and one curved surface. In order to verify that the curvature of the moulds is unimportant, an alternative model will now include the curvature of both moulds. To facilitate this, the system is reconsidered in polar coordinates, using the standard change of coordinates. Now, there is only one length scale, the radial distance r from the centre of the circular part of the lower mould. The small parameter arises from the ratio of a typical radial distance from the upper mould to the centre, to the difference between r_1 and this typical distance.

The governing equations are the Navier-Stokes equations in polar coordinates (see Acheson, 1990, p. 353), along with no-slip and no-flow boundary conditions.

To nondimensionalise the equations, the variables are scaled as follows:

$$r = R(1+\varepsilon_p r'), \quad t = \frac{\varepsilon_p R}{v_0} t', \quad u_r = v_0 u_r', \quad u_\theta = \frac{v_0}{\varepsilon_p} u_\theta', \quad p = \frac{\rho {v_0}^2}{\varepsilon_p^4 \mathrm{Re}_p} p', \quad Q = v_0 R Q', \tag{41}$$

where figure 5 shows how r is formulated and $R = r_1 - 3h_0$, $\varepsilon_p = \frac{r_1 - R}{R} \approx 0.09 \ll 1$ is a small parameter, and $\mathrm{Re}_p = v_0 \rho R / \varepsilon_p \mu$ is the Reynolds number for the polar coordinate model.

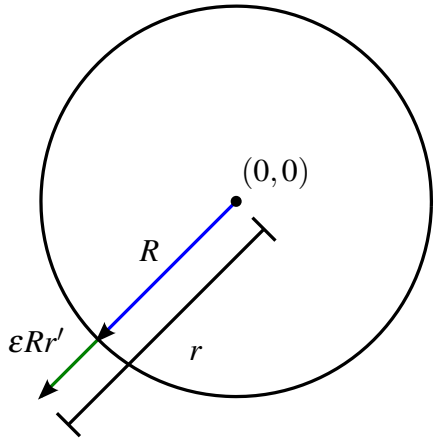

Figure 5: Schematic showing how r is nondimensionalised, $r = R(1+\varepsilon_p r')$. The constant R is chosen to be a representative radial distance. This figure is not drawn to scale.

Nondimensionalising the polar Navier-Stokes equations, taking terms to $O(\varepsilon_p)$ and dropping the $(\cdot)'$ notation give

$$0 = \frac{\partial p}{\partial r}, \tag{42}$$

$$0 = \frac{\partial u_r}{\partial r} + \varepsilon_p \frac{\partial (r u_r)}{\partial r} + \frac{\partial u_\theta}{\partial \theta}, \tag{43}$$

$$\frac{\partial p}{\partial \theta} = \frac{\partial}{\partial r}\left((1+\varepsilon_p r) \frac{\partial u_\theta}{\partial r} \right). \tag{44}$$

In dimensionless terms, the boundary conditions are

$$u_r = u_\theta = 0 \quad \text{on} \quad r = C_1(\theta), \tag{45}$$

$$u_\theta = -\varepsilon_p \cos\theta, u_r = -\sin\theta \quad \text{on} \quad r = C_2(t,\theta), \tag{46}$$

and the conditions at the free surfaces, $\theta = \theta_i$, are

$$p(t,\theta_i) = 0, \quad Q(t,\theta_i) = \left(C_1(\theta_i) - C_2(t,\theta_i) + \frac{\varepsilon_p}{2}\left(C_1^2(\theta_i) - C_2^2(t,\theta_i)\right)\right)\dot{\theta}_i, \tag{47}$$

for $i = 1,2$. These conditions are analogous to (33). Please see appendix B.2 for a detailed description of the equations of the mould surfaces in polar coordinates.

The first thin film equation, (42), implies that

$$p = p(t,\theta). \tag{48}$$

This means that the pressure is independent of the radial coordinate. This allows for equation (44) to be integrated once with respect to r to give

$$(1+\varepsilon_p r)\frac{\partial u_\theta}{\partial r} = \frac{\partial p}{\partial \theta} r + A(t,\theta), \tag{49}$$

which upon rearranging is equivalent to

$$\frac{\partial u_\theta}{\partial r} = \frac{1}{1+\varepsilon_p r}\left(\frac{\partial p}{\partial \theta} r + A(t,\theta)\right), \tag{410}$$

where A is an unknown function of integration. Taking a Taylor series around $\varepsilon_p = 0$, (410) is approximated to

$$\begin{aligned}\frac{\partial u_\theta}{\partial r} &\approx (1-\varepsilon_p r)\left(\frac{\partial p}{\partial \theta} r + A(t,\theta)\right) \\ &= \left(\frac{\partial p}{\partial \theta} - \varepsilon_p A(t,\theta)\right) r - \varepsilon_p \frac{\partial p}{\partial \theta} r^2 + A(t,\theta).\end{aligned} \tag{411}$$

Integrating one more time leads to an expression for u_θ,

$$u_\theta = \left(\frac{\partial p}{\partial \theta} - \varepsilon_p A(t,\theta)\right)\frac{r^2}{2} - \varepsilon_p \frac{\partial p}{\partial \theta}\frac{r^3}{3} + A(t,\theta) r + B(t,\theta), \tag{412}$$

where B is a second unknown function of integration. Applying condition (45) fixes B in terms of A:

$$B(t,\theta) = -\left(\frac{\partial p}{\partial \theta} - \varepsilon_p A(t,\theta)\right)\frac{C_1^2}{2} + \varepsilon_p \frac{\partial p}{\partial \theta}\frac{C_1^3}{3} - A(t,\theta) C_1. \tag{413}$$

To find A, condition (46) is applied to give:

$$A = \frac{\frac{\varepsilon_p}{3}\frac{\partial p}{\partial \theta}(C_2^3 - C_1^3) - \frac{1}{2}\frac{\partial p}{\partial \theta}(C_2^2 - C_1^2) - \varepsilon_p \cos\theta}{C_2 - C_1 - \frac{\varepsilon_p}{2}(C_2^2 - C_1^2)}$$
$$= \frac{\frac{\varepsilon_p}{3}\frac{\partial p}{\partial \theta}(C_1^2 + C_1C_2 + C_2^2) - \frac{1}{2}\frac{\partial p}{\partial \theta}(C_1 + C_2) - \frac{\varepsilon_p \cos\theta}{(C_2 - C_1)}}{1 - \frac{\varepsilon_p}{2}(C_1 + C_2)}, \tag{414}$$

which again can be approximated by taking a Taylor expansion around $\varepsilon_p = 0$ and retaining only $\mathrm{O}(\varepsilon_p)$ terms:

$$A = \left[\frac{\varepsilon_p}{3}\frac{\partial p}{\partial \theta}(C_1^2 + C_1C_2 + C_2^2) - \frac{1}{2}\frac{\partial p}{\partial \theta}(C_1 + C_2) - \frac{\varepsilon_p \cos\theta}{C_2 - C_1}\right]$$
$$\times \left[1 + \frac{\varepsilon_p}{2}(C_1 + C_2)\right] + \mathrm{O}(\varepsilon_p^2)$$
$$\approx -\frac{1}{2}\frac{\partial p}{\partial \theta}(C_1 + C_2) + \frac{\varepsilon_p}{12}\frac{\partial p}{\partial \theta}(C_2 - C_1)^2 - \frac{\varepsilon_p \cos\theta}{C_2 - C_1}. \tag{415}$$

Substituting the expressions for A, (415), and B, (413), into (412), results in an expression for the angular component of velocity,

$$u_\theta = (r - C_1)\left[-\frac{1}{2}\frac{\partial p}{\partial \theta}(C_1 + C_2) + \frac{\varepsilon_p}{12}\frac{\partial p}{\partial \theta}(C_2 - C_1)^2 - \varepsilon_p \frac{\cos\theta}{C_2 - C_1}\right]$$
$$+ \frac{r^2 - C_1^2}{2}\left[\frac{\partial p}{\partial \theta} + \frac{\varepsilon_p}{2}\frac{\partial p}{\partial \theta}(C_1 + C_2)\right] - \varepsilon_p \frac{r^3 - C_1^3}{3}\frac{\partial p}{\partial \theta} + \mathrm{O}(\varepsilon_p^2). \tag{416}$$

Now, the flux, Q, can be calculated by

$$Q = \int_{C_2}^{C_1} u_\theta \, \mathrm{d}r, \tag{417}$$

and via (416), we obtain

$$Q = \frac{\varepsilon_p}{2}\cos\theta(C_2 - C_1) + \frac{1}{24}\frac{\partial p}{\partial \theta}(C_1 - C_2)^3(\varepsilon_p C_1 - 2 + \varepsilon_p C_2). \tag{418}$$

By conservation of mass of the fluid, the flux satisfies

$$\frac{\partial Q}{\partial \theta} = \frac{\partial C_2}{\partial t}(1 + \varepsilon_p C_2), \tag{419}$$

and integrating over θ gives

$$Q = \int \frac{\partial C_2}{\partial t}(1+\varepsilon_p C_2)\,\mathrm{d}\theta + \phi(t), \tag{420}$$

where $\phi(t)$ is as yet unknown. Setting (418) equal to (420), isolating $\frac{\partial p}{\partial \theta}$, integrating over θ and using the first condition in (47) fixes ϕ to be

$$\phi(t) = -\frac{\displaystyle\int_{\theta_1}^{\theta_2} \frac{\varepsilon_p \cos\theta}{2(C_1-C_2)^2(\varepsilon_p C_1 - 2 + \varepsilon_p C_2)}\,\mathrm{d}\theta + \int_{\theta_1}^{\theta_2} \frac{\int \frac{\partial C_2}{\partial t}(1+\varepsilon_p C_2)\,\mathrm{d}\theta}{(C_1-C_2)^3(\varepsilon_p C_1 - 2 + \varepsilon_p C_2)}\,\mathrm{d}\theta}{\displaystyle\int_{\theta_1}^{\theta_2} \frac{1}{(C_1-C_2)^3(\varepsilon_p C_1 - 2 + \varepsilon_p C_2)}\,\mathrm{d}\theta}. \tag{421}$$

To obtain ODEs for the fluid boundaries, θ_1 and θ_2, we examine the volume of fluid, V, where

$$V = \int_{\theta_1}^{\theta_2} C_1 - C_2 + \frac{\varepsilon_p}{2}(C_1^2 - C_2^2)\,\mathrm{d}\theta. \tag{422}$$

Conserving the volume of fluid, by setting $\frac{\mathrm{d}V}{\mathrm{d}t} = 0$, gives

$$\begin{aligned} 0 = {} & \dot{\theta}_2 \left(C_1(\theta_2) - C_2(t,\theta_2) + \frac{\varepsilon_p}{2}\left(C_1^2(\theta_2) - C_2^2(t,\theta_2)\right)\right) \\ & - \dot{\theta}_1 \left(C_1(\theta_1) - C_2(t,\theta_1) + \frac{\varepsilon_p}{2}\left(C_1^2(\theta_1) - C_2^2(t,\theta_1)\right)\right) \\ & + \int_{\theta_1}^{\theta_2} \frac{\partial}{\partial t}\left(C_1(\theta) - C_2(t,\theta) + \frac{\varepsilon_p}{2}\left(C_1^2(\theta) - C_2^2(t,\theta)\right)\right)\mathrm{d}\theta. \end{aligned} \tag{423}$$

Separating (423) into θ_1 and θ_2 terms gives

$$\begin{aligned} \dot{\theta}_2 \left[C_1(\theta_2) - C_2(t,\theta_2) + \frac{\varepsilon_p}{2}\left(C_1^2(\theta_2) - C_2^2(t,\theta_2)\right)\right] - \int_0^{\theta_2} \frac{\partial C_2(t,\theta)}{\partial t}\left(1+\varepsilon_p C_2(t,\theta)\right)\mathrm{d}\theta \\ = \dot{\theta}_1 \left[C_1(\theta_1) - C_2(t,\theta_1) + \frac{\varepsilon_p}{2}\left(C_1^2(\theta_1) - C_2^2(t,\theta_1]\right)\right] \\ - \int_{\theta_1}^{0} \frac{\partial C_2(t,\theta)}{\partial t}\left(1+\varepsilon_p C_2(t,\theta)\right)\mathrm{d}\theta \equiv \Omega(t), \end{aligned} \tag{424}$$

where $\Omega(t)$ is some unknown function. Comparing (424) to (420), and noting (47), it can be seen that $\Omega(t) = \phi(t)$. The evolutions of the fluid boundaries are

therefore described by two ODEs,

$$\dot{\theta}_1(t) = \frac{\phi(t) + \int \frac{\partial C_2}{\partial t}(1+\varepsilon_p C_2)\,\mathrm{d}\theta\big|_{\theta_1}}{C_1(\theta_1) - C_2(t,\theta_1) + \frac{\varepsilon_p}{2}(C_1^2(\theta_1) - C_2^2(t,\theta_1))}, \tag{425}$$

$$\dot{\theta}_2(t) = \frac{\phi(t) + \int \frac{\partial C_2}{\partial t}(1+\varepsilon_p C_2)\,\mathrm{d}\theta\big|_{\theta_2}}{C_1(\theta_2) - C_2(t,\theta_2) + \frac{\varepsilon_p}{2}(C_1^2(\theta_2) - C_2^2(t,\theta_2))}. \tag{426}$$

As in section 3, the initial conditions for θ_1 and θ_2 are determined numerically. This is done by choosing a value for θ_{cm} at t_0, the initial time, and then $\theta_1(t_0)$ and $\theta_2(t_0)$ are found such that they satisfy a given constant volume, V_0.

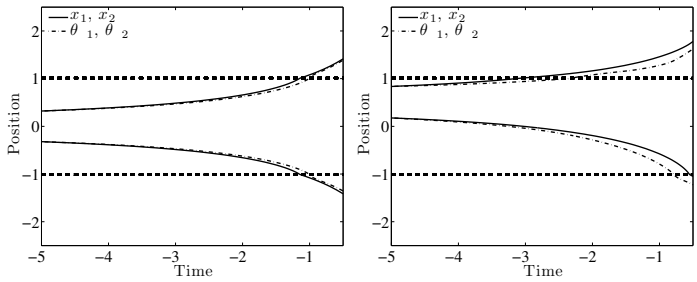

(a) $x_{\mathrm{cm}}(t_0) = 0$. (b) $x_{\mathrm{cm}}(t_0) = 0.5$.

Figure 6: Evolution of the fluid boundaries for the polar model, overlaid with the simple case.

4.1 Numerical results

Figure 6 displays the numerical solutions for the system of ODEs given in section 4 along with the results obtained in section 3. Comparing the figures, there is no qualitative difference between the two sets of results. The difference in the evolution of the free surfaces is more marked for the case when $x_{\mathrm{cm}}(t_0) = 0.5$, shown in figure 6b. The free surfaces for both the simple and polar models move out asymmetrically. As the height between the moulds decreases the difference in the positions of the free surfaces for the two cases becomes more pronounced. While this difference exists, overall the evolution of the free surfaces is very similar and qualitatively, the two models produce the same results.

This validates the use of the flat model in section 3. It also helps to explain why the fluid remains off-centred once it begins so. From the perspective of the

fluid, the moulds appear flat, therefore when the upper mould is pushed down on the fluid it is squeezed out in both directions from its initial position. There is no mechanism available for it to overcome its off-centredness.

5 Model adjustments

5.1 Including surface tension

In section 3, (33) assumes that the pressure at the free surfaces of the fluid boundaries is zero. If the effects of surface tension are included, this assumption is no longer valid. The integral of equation (39) is now

$$\int_{x_1}^{x_2} \frac{\partial p}{\partial x}\,\mathrm{d}x = p(t,x_2) - p(t,x_1) = \Delta p. \tag{51}$$

Therefore, the position of maximum pressure, x_0, is

$$x_0 = \frac{\frac{\Delta p}{12} + \int_{x_1}^{x_2} \frac{x}{h(t,x)^3}\,\mathrm{d}x}{\int_{x_1}^{x_2} \frac{1}{h(t,x)^3}\,\mathrm{d}x}. \tag{52}$$

To find Δp approximately, we use the dimensional Young-Laplace equation, given by

$$p = \frac{\gamma}{r_0}, \tag{53}$$

where γ is the surface tension and r_0 is the radius of curvature of the fluid boundary. A contact angle of 180° is assumed to see the maximum effect surface tension would have on the dynamics. After nondimensionalising, the difference in pressure is

$$\Delta p \approx 2\lambda \left(\frac{1}{h(t,x_2)} - \frac{1}{h(t,x_1)} \right), \tag{54}$$

where $\lambda = \frac{\varepsilon^2 \gamma}{v_0 \mu}$ is a reduced inverse capillary number, ($\lambda = \frac{\varepsilon^2}{\mathrm{Ca}}$, where Ca is the capillary number). Note that the pressure difference is proportional to ε^2, indicating that the effect of including surface tension will be negligible unless $\mathrm{Ca} = O(\varepsilon^2)$ or smaller.

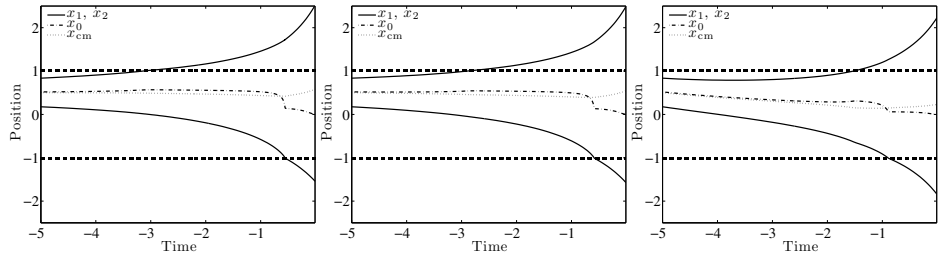

(a) $x_{cm} = 0.5\,, \lambda = 0$ (b) $x_{cm} = 0.5\,, \lambda = 0.1$ (c) $x_{cm} = 0.5\,, \lambda = 1$

Figure 7: Effects of including surface tension.

5.1.1 Numerical results

Equation (52) is substituted in the place of equation (310) and the system is solved as in section 3. Figure 7 shows the numerical solutions. Figure 7a, where $\lambda = 0$, has no surface tension (the case seen previously in figure 4b). Upon increasing λ to 0.1, figure 7b, there is no discernible difference between that and the $\lambda = 0$ case. However, if λ is increased to 1, as in figure 7c, a difference in dynamics is observable.

When the effect of surface tension is amplified, the free surface of the fluid at the boundary furthest from $x = 0$ (x_2 in this case) has a smaller radius of curvature than the other fluid boundary and so experiences a greater pressure. This results in the fluid at this side being initially pushed back to the centre. This movement helps to centre the fluid and it can be seen in figure 7c that the fluid boundaries reach the flat parts of the moulds almost simultaneously.

The parameter range particular to this setup is $0 < \lambda \ll 1$. Hence surface tension plays no role in the dynamics of the fluid flow and can, justifiably, be neglected from the model. However, if the system could be altered to increase the effect of surface tension, it would reduce the amount of asymmetrical flow. This could be done by using a less viscous fluid or by moving the upper mould more slowly. If the parameters v_0 and μ were reduced to 0.06 mm s^{-1} and 0.25 Pa s, respectively, the system would experience the effect of surface tension. The benefit of this would need to be weighed against the slower timescale and the cost of altering the fluid.

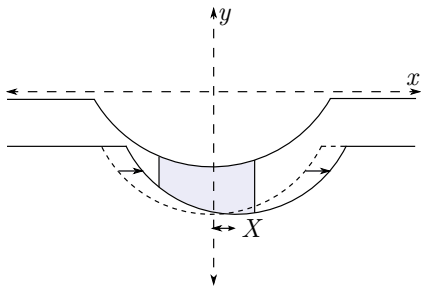

Figure 8: Geometry of the moulds and positions of the fluid boundaries.

5.2 Including mould misalignment

In the previous sections, the lower mould is fixed in place. This condition reflects the manufacturing setup where the lower mould does not move. One of the questions posed at the outset of this study was whether allowing the lower mould to move laterally would decrease the amount of asymmetric flow of fluid between the moulds, by allowing an initially off-centred fluid dose to centre itself. This would, in turn, reduce the number of discarded contact lenses, saving a manufacturer resources and money. To investigate this suggestion, the lower mould will now be allowed to move horizontally, as in figure 8. Included in this setup is the possibility of an initial offset between the lower and upper moulds. The offset, i.e. the horizontal distance from the centre of the bottom mould to the centre of the upper mould is denoted $X(t)$ and the rate of change of X is denoted $\dot{X}$. In order to simplify the algebra, the boundaries are now such that the upper mould is at $y = 0$, and the lower mould is $y = -h(t,x,X)$, where the height between moulds, h, now also depends on X. Solving the thin film equations, for the new system yields

$$u = \frac{1}{2}\frac{\partial p}{\partial x}(y^2 + hy) - \frac{\dot{X}}{h}y, \tag{55}$$

the velocity in the x-direction. Integrating u over the height of fluid gives the flux,

$$Q = \int_{-h}^{0} u \,\mathrm{d}y = -\frac{1}{12}\frac{\partial p}{\partial x}h^3 + \frac{\dot{X}h}{2}. \tag{56}$$

The volume of fluid is

$$V = \int_{x_1}^{x_2} h(t,x,X)\,\mathrm{d}x. \tag{57}$$

To obtain ODEs for the fluid boundaries, conservation of volume is considered:

$$\frac{\mathrm{d}V}{\mathrm{d}t} = \dot{x}_2 h(t,x_2,X) - \dot{x}_1 h(t,x_1,X) + \int_{x_1}^{x_2} \left(\frac{\partial h}{\partial t} + \dot{X} \frac{\partial h}{\partial X} \right) \mathrm{d}x, \tag{58}$$

$$= \dot{x}_2 h(t,x_2,X) - \dot{x}_1 h(t,x_1,X) - x_2 + x_1 + \dot{X} \int_{x_1}^{x_2} \frac{\partial h}{\partial X} \mathrm{d}x. \tag{59}$$

However, using $h = C_2(t,x) - C_1(x,X)$ and exploiting the fact that $C_1(x,X) = C_1(x-X)$ gives

$$\frac{\partial h}{\partial X} = \frac{\partial C_1}{\partial x}, \tag{510}$$

and hence the rate of change of volume may be written

$$\frac{\mathrm{d}V}{\mathrm{d}t} = \dot{x}_2 h(t,x_2,X) - \dot{x}_1 h(t,x_1,X) - x_2 + x_1 + \dot{X} C_1(x_2,X) - \dot{X} C_1(x_1,X) = 0. \tag{511}$$

Equation (511) can be grouped into x_1 and x_2 terms:

$$\dot{x}_1 h(t,x_1,X) - x_1 + \dot{X} C_1(x_1,X) = \dot{x}_2 h(t,x_2,X) - x_2 + \dot{X} C_1(x_2,X) = F(t,X), \tag{512}$$

where F is some unknown function. Conservation of mass yields

$$-\frac{\partial Q}{\partial x} = \frac{\partial h}{\partial t} + \dot{X} \frac{\partial C_1}{\partial x}, \tag{513}$$

and given that $\frac{\partial h}{\partial t} = -1$ and integrating over x gives

$$Q + \dot{X} C_1 = x - x_0(t,X). \tag{514}$$

Substituting (56) into (514) leads to

$$\frac{\partial p}{\partial x} = \frac{12}{h^3} \left(\dot{X} \left(\frac{h}{2} + C_1 \right) - x + x_0 \right). \tag{515}$$

For this model, equation (33) holds and so,

$$x_0(t,X) = \frac{\displaystyle\int_{x_1}^{x_2} \frac{x}{h^3} \mathrm{d}x - \dot{X} \int_{x_1}^{x_2} \left(\frac{1}{2h^2} + \frac{C_1}{h^3} \right) \mathrm{d}x}{\displaystyle\int_{x_1}^{x_2} \frac{1}{h^3} \mathrm{d}x}, \tag{516}$$

which for simplicity we will write $x_0 = I_1 - \dot{X} I_2$, where

$$I_1 = \frac{\int_{x_1}^{x_2} \frac{x}{h^3}\,\mathrm{d}x}{\int_{x_1}^{x_2} \frac{1}{h^3}\,\mathrm{d}x}, \qquad I_2 = \frac{\int_{x_1}^{x_2} \left(\frac{1}{2h^2} + \frac{C_1}{h^3}\right)\mathrm{d}x}{\int_{x_1}^{x_2} \frac{1}{h^3}\,\mathrm{d}x}. \tag{517}$$

Comparing (512) and (514), and given that $Q(t,X,X) = \dot{x}h(t,x,X)$ at the boundaries, we see that

$$F(t,X) = -x_0(t,X), \tag{518}$$

and therefore, the ODEs for the evolution of the boundaries are

$$\dot{x}_1 = \frac{x_1 - x_0 - \dot{X} C_1(x_1,X)}{h(t,x_1,X)}, \tag{519}$$

$$\dot{x}_2 = \frac{x_2 - x_0 - \dot{X} C_1(x_2,X)}{h(t,x_2,X)}. \tag{520}$$

The next step is to find an expression for $\dot{X}$. If the lower mould is allowed to move, it may potentially become offset to the extent that it comes into contact with the upper mould. There are two cases: the first case where the lower and upper moulds may or may not be in contact but the velocity of the lower mould depends on the dynamics of the fluid, $\dot{X} = \dot{X}_f$; and the second case where the lower and upper moulds are in contact and the velocity of the lower mould depends on its position, $\dot{X} = \dot{X}_c$. Due to the geometry of the moulds, the point of contact will always be at one of the corners on the lower mould and somewhere on the curved part of the upper mould, so that $-1 < x_c < 1$, where x_c is the point of contact. There is no fluid at the point of contact. Regardless of whether or not the moulds are in contact, the upper mould moves downwards at a constant speed until $t = 0$.

To find $\dot{X}_f$ we consider conservation of momentum along $y = -h$,

$$\int_{x_1}^{x_2} \mathbf{x} \cdot \boldsymbol{\sigma} \cdot \mathrm{d}\mathbf{S} = 0, \tag{521}$$

where $\mathbf{x}$ is the position vector, $\boldsymbol{\sigma}$ is the stress tensor and $\mathbf{S}$ is the surface. To $O(1)$, (521) is

$$\int_{x_1}^{x_2} p\frac{\partial C_1}{\partial x} + \left.\frac{\partial u}{\partial y}\right|_{-h} \mathrm{d}x = 0, \tag{522}$$

where the first term in the integrand represents the pressure from the fluid pushing the mould and the second term represents the fluid's resistance to shearing. Via

integration by parts of the first term, (522) becomes

$$\int_{x_1}^{x_2} -C_1 \frac{\partial p}{\partial x} + \left.\frac{\partial u}{\partial y}\right|_{-h} \mathrm{d}x = 0, \tag{523}$$

and substituting (55) and (515), and rearranging leads to an expression for $\dot{X}_f$:

$$\dot{X}_f = \frac{3\displaystyle\int_{x_1}^{x_2} \frac{(x-I_1)}{h^2}\left(\frac{2C_1}{h}+1\right)\mathrm{d}x}{\displaystyle\int_{x_1}^{x_2} 3\frac{(C_1-I_2)}{h^2}\left(\frac{2C_1}{h}+1\right)+\frac{1}{h}\left(\frac{3C_1}{h}+2\right)\mathrm{d}x}. \tag{524}$$

When the lower mould moves with velocity $\dot{X} = \dot{X}_c$, we assume that the lower mould slips along the upper mould so that they remain in contact. That is

$$\dot{X}_c = \left(\frac{\partial C_1}{\partial x}\right)^{-1} = \frac{\varepsilon}{x_c}\sqrt{\left(\frac{r_2}{b}\right)^2 - x_c^2}, \tag{525}$$

where x_c is the point of contact. When the moulds are in contact, the lower mould will move with velocity $\dot{X}_c$ unless $\dot{X}_f$ is such that it pushes the moulds apart. This can be summed up succinctly by two inequalities. If

$$X\dot{X} < 0, \tag{526}$$

and

$$|\dot{X}_f| > |\dot{X}_c|, \tag{527}$$

then the lower mould will move with velocity $\dot{X}_f$. Otherwise, the lower mould will move with velocity $\dot{X}_c$. This allows the moulds to come into contact but be pushed apart again by the fluid.

5.2.1 Numerical results

To solve the system described in section 5.2, the initial value for the misalignment, $X(t_0)$, must be specified. The left column of figure 9 displays the evolution of the fluid boundaries for several combinations of $x_{\mathrm{cm}}(t_0)$ and $X(t_0)$. The graphs also show the evolution of X and x_{cm}. The right column of figure 9 displays X in more detail.

Figures 9a and 9b show the case where the lower mould is offset to the right ($X(t_0) = 0.1$) while the initial dose is to the left ($x_{\mathrm{cm}}(t_0) = -0.2$). The pressure

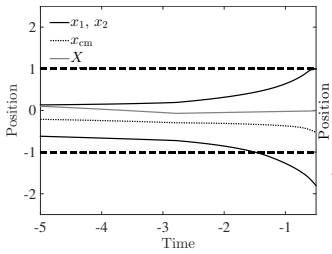

(a) Case 1: $x_{\text{cm}} = -0.2, X = 0.1$

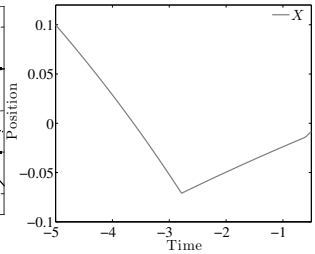

(b) Case 1: $x_{\text{cm}} = -0.2, X = 0.1$

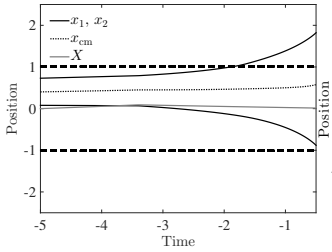

(c) Case 2: $x_{\text{cm}} = 0.4, X = 0$

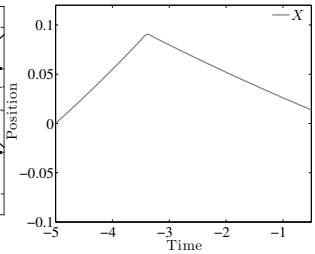

(d) Case 2: $x_{\text{cm}} = 0.4, X = 0$

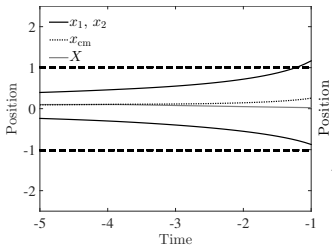

(e) Case 3: $x_{\text{cm}} = 0.1, X = 0.1$

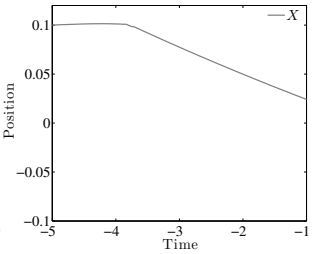

(f) Case 3: $x_{\text{cm}} = 0.1, X = 0.1$

Figure 9: Left column: Evolution of the fluid boundaries. Right column: Evolution of the offset of the lower mould.

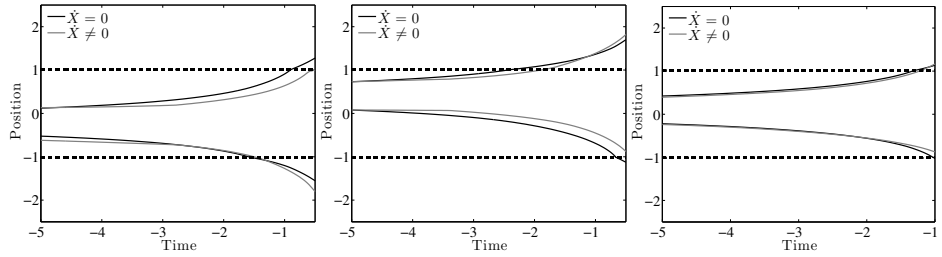

(a) $x_{\text{cm}} = -0.2, X = 0.1$ (b) $x_{\text{cm}} = 0.4, X = 0$ (c) $x_{\text{cm}} = 0.1, X = 0.1$

Figure 10: Comparison of regular case to misaligned case.

from the fluid pushes the lower mould to the left, so much so that it becomes negatively offset. At $t \approx -2.8$ the lower mould comes into contact with the upper mould and slides along it until at $t \approx -0.6$ when the moulds come apart again. This can be seen in the change of slope of X.

Figures 9c and 9d show the case where there is no initial offset of the lower mould ($X(t_0) = 0$) but the dose of fluid is initially positioned to the right ($x_{\text{cm}}(t_0) = 0.4$). This positioning of the fluid causes the lower mould to move to the right. Again, it makes contact with the upper mould at $t \approx -3.3$ and then slides back to its central position.

In the last case, figures 9e and 9f, both the initial position of the lower mould and the initial dose of fluid are to the right ($X(t_0) = x_{\text{cm}}(t_0) = 0.1$). The dynamics of the fluid do not have much influence on the position of the lower mould and it remains stable at $X = 0.1$. At $t \approx -3.7$ the upper mould has moved down to the point where the moulds make contact. The lower mould then slides along the upper mould until it has reached the central position.

In this section, lateral movement of the lower mould was introduced to the model. At the outset of the study, it was thought that this would improve on the results from section 3. Including lateral movement of the lower mould complicates the dynamics of the fluid. A feedback loop is established, with the position of the lower mould affecting the motion of the fluid and the dynamics of the fluid influencing the offset of the lower mould.

It is not entirely correct to compare the case where there is no movement of the lower mould and the case where there is, as the only time the initial conditions are the same is when there is no offset of the lower mould. However, for qualitative results, figure 10 shows an overlay of the two cases. In all three cases, allowing the bottom mould to move increases the time taken for both fluid boundaries to

reach the flat part of the moulds. The time taken for both fluid boundaries to reach the the flat part of the moulds is an indicator for the amount of asymmetry in the system. The time is minimised when the fluid is perfectly centred and increases as the amount of asymmetry increases. Therefore, the results in this section indicate that allowing for lateral movement of the lower mould increases asymmetrical flow. While the results shown are not proof that it would be the same for all initial values of X and x_{cm}, they do point to that being the case.

6 Conclusions

Pressure moulding of contact lenses, modelled as a viscous fluid squeezed between two spherical surfaces, was studied using a simple mathematical model. A first case, where one of the surfaces was treated as flat, was compared to a more realistic model with two curved surfaces. However, as demonstrated, there is no fundamental difference in the motion of the fluid between the two cases and hence the simple model may be used to accurately describe the dynamics of the fluid.

It was shown that if the fluid is originally centred in the moulds it will remain so. Similarly, if the fluid is originally off-centred, it will stay off-centred. This demonstrates that there is no mechanism for the fluid to centre itself once it begins off-centred. Consequently, for manufacturing purposes it is important to ensure that the initial positioning of the fluid is as accurate as possible.

Variations on the simple model were explored. Including surface tension effects was shown to have no influence on the flow in the parameter range of interest. It is possible that at lower volumes of fluid the effect could be increased due to the boundaries having smaller radii of curvature.

Allowing the lower mould to move complicates the dynamics of the fluid. Although not all possible initial conditions of the alignment were examined, three representative cases showed that the time taken for both fluid boundaries to pass out of the circular region increased when the lower mould had the ability to move. This indicates that asymmetrical flow is increased when lateral movement of the lower mould is allowed. Therefore to ensure symmetrical flow it is recommended that the lower mould is kept fixed in place.

The authors acknowledge the support of the Mathematics Applications Consortium for Science and Industry (www.macsi.ul.ie) funded by the Science Foundation Ireland mathematics initiative grant 06/MI/005 and the support of the Embark Scholarship funded by the Irish Research Council.

A Stability of $x_0(t)$

In this appendix, the stability of $x_0(t)$ is investigated. To do this, it is assumed that $x_0(t)$, the position of maximum pressure, is small, $x_0(t) \ll 1$, and a linear expansion of $\dot{x}_0(t)$ around $x_0 = 0$ is considered. As stated in equation (310), $x_0(t)$ is given by

$$x_0(t) = \frac{\int_{x_1}^{x_2} \frac{x}{h^3}\,\mathrm{d}x}{\int_{x_1}^{x_2} \frac{1}{h^3}\,\mathrm{d}x}, \tag{A1}$$

where $x_1(t)$ and $x_2(t)$ are the positions of the free surfaces of the fluid and their evolution is given by

$$\dot{x}_1(t) = \frac{x_1(t) - x_0(t)}{h(t, x_1(t))}, \tag{A2}$$

$$\dot{x}_2(t) = \frac{x_2(t) - x_0(t)}{h(t, x_2(t))}. \tag{A3}$$

Differentiating $x_0(t)$ and substituting equations (A2) and (A3) gives

$$\dot{x}_0(t) = \frac{\int_{x_1}^{x_2} \frac{3x}{h^4}\,\mathrm{d}x + \left.\frac{x^2}{h(t,x(t))^4}\right|_{x_1}^{x_2}}{\int_{x_1}^{x_2} \frac{1}{h^3}\,\mathrm{d}x} + x_0 \frac{\left(\left.\frac{-2x}{h(t,x(t))^4}\right|_{x_1}^{x_2} - \int_{x_1}^{x_2} \frac{3}{h^4}\,\mathrm{d}x\right)}{\int_{x_1}^{x_2} \frac{1}{h^3}\,\mathrm{d}x} + O(x_0^2). \tag{A4}$$

To examine the stability of x_0, the time domain is split into two parts: the time before x_1 and x_2 have both reached the flat part of the moulds ($|x_i| < a$, $i = 1$ or 2); and the time after that. In the first case, equation (A4) can be expressed as

$$\dot{x}_0 = x_0 f_1(t), \tag{A5}$$

where f_1 can be found numerically.

In the second case, when both free surfaces are past the curved part of the mould ($|x_i| > a$, $i = 1, 2$) the height of the fluid at these points is equal,

$$h(t, x_1) = h(t, x_2) \equiv H(t). \tag{A6}$$

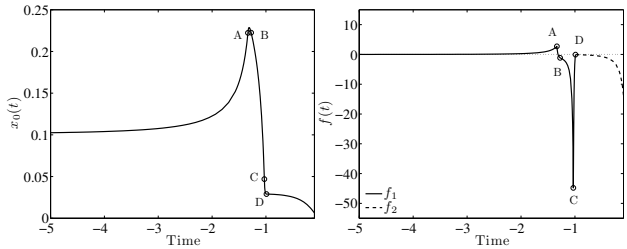

(a) $x_0(t)$. (b) $f(t)$.

Figure 11: Position of maximum pressure, $x_0(t)$, on the left and its stability, $f(t)$, on the right, for the particular case of $x_{\text{cm}}(t_0) = 0.1$. The stability, f, is defined in two parts: $f = f_1$ when one or both of the free surfaces have not reached the flat part of the mould and $f = f_2$ when both free surfaces are in the flat region of the mould. The circles mark times of interest as follows. A: $x_2 = 1$; B: $x_2 = a$; C: $x_1 = -1$; D: $x_1 = -a$.

Exploiting this, equation (A4) can be written as

$$\dot{x}_0(t) = x_0 \underbrace{\left(\frac{5}{H(t)} + \frac{\dfrac{2(x_1 - x_2)}{H(t)^4} - \displaystyle\int_{x_1}^{x_2} \frac{3}{h^4}\,\mathrm{d}x}{\displaystyle\int_{x_1}^{x_2} \frac{1}{h^3}\,\mathrm{d}x} \right)}_{=f_2(t)}, \tag{A7}$$

where $f_2(t) < 0$. Taking these two cases together gives

$$\frac{\dot{x_0}(t)}{x_0(t)} = f(t) = \begin{cases} f_1(t) & \text{if } |x_i| < a,\ i = 1 \text{ or } 2, \\ f_2(t) & \text{otherwise.} \end{cases} \tag{A8}$$

Figure 11 shows the numerical calculations of $x_0(t)$ and $f(t)$ for $x_{\text{cm}} = 0.1$. When $f(t)$ is positive, x_0 is unstable, when $f(t)$ is negative, x_0 is stable and when $f(t)$ is equal to zero it is neutrally unstable. The circles on the graph mark certain times of interest. Point A marks the time when $x_2 = 1$. Point B marks the time when $x_2 = a$, that is, the right fluid boundary has passed into the flat part of the moulds. Point C marks when $x_1 = -1$ and point D marks the time when $x_1 = -a$, and so from this point onwards both fluid boundaries are in the flat part of the mould.

Therefore, $f_1(t)$ is the section of the curve from $t = t_0$ to point D, shown by the blue line in figure 11, and $f_2(t)$ is the section of the curve from point D to $t = 0$, shown by the green line.

Until $t \approx -2$, f_1 is positive but very small ($f_1 \ll 1$). This implies that the system is marginally stable here. An off-centred dose is pushed away from the centre by a negligible amount. This behaviour can be seen in figure 11a, where x_0 remains close to its starting point. At point A, f_1 reaches its maximum and is no longer small. However, $\int_{t_0}^{t_{\text{flat}}} f_1 \, \mathrm{d}t \ll 1$ and so the magnitude of the instability is small, where t_{flat} is the time until both fluid boundaries are in the flat region of the mould. After point A, f_1 quickly becomes negative and remains negative. As mentioned above, f_2 is also negative and therefore the system is stable for the remainder of the time period.

This stability analysis shows that for part of the evolution of the system it is unstable, however that instability is too small to affect its dynamics significantly.

B Equations of the mould surfaces

In this appendix, the dimensional equations for the lower and upper moulds are given in Cartesian and polar coordinates.

B.1 Cartesian Coordinates

In Cartesian coordinates, the dimensional lower mould, $C_1(x)$, is

$$C_1(x) = \begin{cases} -\sqrt{r_1^2 - x^2} & \text{if} \quad -b \leqslant x \leqslant b \\ -\sqrt{r_1^2 - b^2} & \text{if} \quad x < -b \quad \text{or} \quad x > b, \end{cases} \tag{B1}$$

where r_1 is the radius of curvature and b is half the horizontal distance of the circular part of the surface, as shown in figure 2. The position of the lower mould is chosen so that the centre of its circular part is at $(x, y) = (0, 0)$.

The dimensional upper mould, $C_2(t, x)$, is

$$C_2(t,x) = \begin{cases} -\sqrt{r_2^2 - x^2} - r_0 + v_0 t & \text{if} \quad -c \leqslant x \leqslant c \\ -\sqrt{r_2^2 - c^2} - r_0 + v_0 t & \text{if} \quad x < -c \quad \text{or} \quad x > c, \end{cases} \tag{B2}$$

where r_2 is the radius of curvature and c is half the horizontal diameter of the circular part of the surface. The position of the upper mould is chosen so that at

$t = 0$ it is in contact with the upper mould at $x = -1$ and $x = 1$. The constant r_0 is defined as

$$r_0 = r_2 - r_1 + h_0, \tag{B3}$$

where $h_0 = h(0,0)$, and lastly

$$v_0 = -\frac{\partial h}{\partial t}, \tag{B4}$$

where v_0 is the velocity of the upper mould.

B.2 Polar Coordinates

In polar coordinates, the dimensional lower mould is

$$C_1(\theta) = \begin{cases} 0 & \text{if} \quad 0 \leqslant \theta \leqslant \pi \quad \text{or} \quad \theta = 2\pi \\ r_1 & \text{if} \quad \alpha_1 < \theta < \alpha_2 \\ -\dfrac{\sqrt{{r_1}^2 - b^2}}{\sin\theta} & \text{if} \quad \pi < \theta \leq \alpha_1 \quad \text{or} \quad \alpha_2 \leqslant \theta < 2\pi, \end{cases} \tag{B5}$$

where α_1 and α_2 are the angles where the upper mould becomes flat and are defined as

$$\alpha_1 = \frac{3\pi}{2} - \sin^{-1}\left(\frac{b}{r_1}\right) \tag{B6}$$

and

$$\alpha_2 = \frac{3\pi}{2} + \sin^{-1}\left(\frac{b}{r_1}\right). \tag{B7}$$

The upper mould is described dimensionally by

$$C_2(t,\theta) = \begin{cases} 0 & \text{if} \quad 0 \leqslant \theta \leqslant \pi \quad \text{or} \quad \theta = 2\pi \\ d(t)\left(\sin\theta + \sqrt{\dfrac{r_2^2}{d(t)^2} - \cos^2\theta}\right) & \text{if} \quad \beta_1 < \theta < \beta_2 \\ \dfrac{d(t) - \sqrt{r_2^2 - c^2}}{\sin\theta} & \text{if} \quad \pi < \theta \leq \beta_1 \quad \text{or} \quad \beta_2 \leqslant \theta < 2\pi, \end{cases} \tag{B8}$$

where

$$\beta_1(t) = \frac{3\pi}{2} - \beta(t), \tag{B9}$$

$$\beta_2(t) = \frac{3\pi}{2} + \beta(t), \tag{B10}$$

and

$$\beta(t) = \tan^{-1}\left(\frac{c}{\sqrt{r_2^2 - c^2} - r_0 + v_0 t}\right). \tag{B11}$$

and $d(t) = r_0 - v_0 t$.

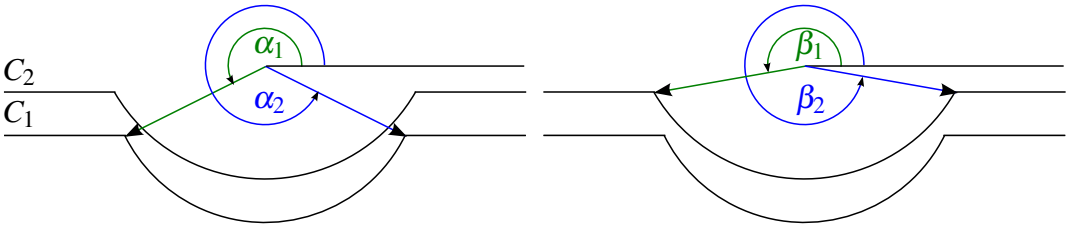

Figure 12: Schematic of the upper and lower moulds in polar coordinates with angles of interest labelled. The figure on the left shows the angles where the lower mould, $C_1(\theta)$, becomes flat. The figure on the right shows the angles where the upper mould, $C_2(t,\theta)$, becomes flat.

References

Acheson, D. J. (1990). *Elementary Fluid Dynamics*. Oxford, UK: Oxford University Press.

Bretherton, F. (1961). The motion of long bubbles in tubes. *Journal of Fluid Mechanics 10*(02), 166–188.

Cameron, A. and C. Mc Ettles (1976). *Basic lubrication theory*. E. Horwood.

Dweib, M. A. and C. M. Ó Bradaigh (2000). Compression moulding of glass reinforced thermoplastics: modelling and experiments. *Polym. Compos. 21*, 832–845.

Engmann, J., C. Servais, and A. S. Burbidge (2005). Squeeze flow theory and applications to rheometry: a review. *J. Non-Newtonian Fluid Mech. 132*, 1–27.

Howell, P. (2003). Surface-tension-driven flow on a moving curved surface. *Journal of engineering mathematics 45*(3-4), 283–308.

Jensen, O. (1997). The thin liquid lining of a weakly curved cylindrical tube. *Journal of Fluid Mechanics 331*, 373–403.

Lawal, A. and D. M. Kalyon (2000). Compressive squeeze flow of generalised Newtonian fluids with apparent wall slip. *Intern. Polym. Process. XV*, 63–71.

Leider, P. J. and R. B. Bird (1974). Squeezing flow between parallel disks. I. Theoretical analysis. *Ind. Eng. Chem. Fund. 13*, 336–341.

Medley, J. B., D. Dowson, and V. Wright (1984). Transient elastohydrodynamic lubrication models for the human ankle joint. *Eng. Med. 13*, 137–151.

Neefe, C. W. (1979). Method of making high quality plastic lenses. *U.S. Patent No. 4,166,088*.

Reynolds, O. (1886). On the theory of lubrication and its application to Mr. Beauchamp Tower's experiments, including an experimental determination of the viscosity of olive oil. *Philos. Trans. R. Soc. London 177*, 157–234.

Roy, R. V., A. J. Roberts, and M. Simpson (2002). A lubrication model of coating flows over a curved substrate in space. *Journal of Fluid Mechanics 454*, 235–261.

Ruggiero, A., E. Gomez, and R. D'Amato (2011). Approximate analytical model for the squeeze-film lubrication of the human ankle joint with synovial fluid filtrated by articular cartilage. *Tribol. Lett. 41*, 337–343.

Stefan, M. (1874). Studies in apparent adhesion (in German). *Sitzber Akad Wiss Wien (Abt II Math Phys) 69*, 713–735.

Talbott, K., A. Xu, D. M. Anderson, and P. Seshaiyer (2014). Modelling the evaporation of a tear film over a contact lens. *Mathematical Medicine and Biology*, dqu001.

Venerus, D. C., M. Kompani, and B. Bernstein (2000). Equibiaxial extensional flow of polymer melts via lubricated squeezing flow. II. Flow modeling. *Rheol. Acta. 39*, 574–582.

Walicki, E. and A. Walicka (2000). Mathematical modelling of some biological bearings. *Smart Mater. Struct. 9*, 280–283.

Yamauchi, A., T. Emi, and S. Seetharaman (2002). A mathematical model for prediction of thickness of mould flux film in continuous casting mould. *ISIJ Int. 42*, 1084–1093.